Eur. Phys. J. D **12**, 235–240 (2000)

THE EUROPEAN PHYSICAL JOURNAL D

EDP Sciences

Realization of a Ramsey-Bordé matter wave interferometer on the K_2 molecule

Ch. Lisdat, M. Frank, H. Knöckel, M.-L. Almazor, and E. Tiemann[a]

Institut für Quantenoptik, Universität Hannover, Welfengarten 1, 30167 Hannover, Germany

Received 13 March 2000

Abstract. We show first results and systematic investigations of a matter wave interferometer with the K_2 molecule, using a transition between the electronic ground state X $^1\Sigma_g^+$ and the state b $^3\Pi(0_u^+)$. This spin forbidden transition is observable due to spin-orbit coupling between the states b and A $^1\Sigma_u^+$. The experimental results are compared with numerical simulations, which show the power of the interferometer to observe small phase shifts by weak interactions.

PACS. 03.75.Dg Atom and neutron interferometry – 42.50.Vk Mechanical effects of light on atoms, molecules, electrons, and ions – 42.62.Fi Laser spectroscopy

1 Introduction

Matter wave interferometers with light-induced beamsplitters are now well established as high precision techniques in spectroscopy [1–4]. Besides the possibility to reduce dramatically the often dominating transit time broadening in the observation of transitions between levels of long lifetimes and to built frequency discriminators with highest stability, the wave character of the studied particles allows many fundamental experiments, for example about influences of topological phases etc.

Although first experiments in this field with molecules [5,6] were already reported, most experiments were and are performed with atoms. We think that molecules promise good perspective in this field due to the higher number of internal degrees of freedom compared to atoms, enlarging the field of possible manipulations of the matter wave. Due to the quantized and addressable level structure of molecules, a large number of systematic investigations can be performed.

The theoretical description of matter wave interferometers is well established [1,3] and will not be recalled here in detail. The wave packet of a moving particle in a molecular beam is split up and recombined (Fig. 1) through a series of absorptions and stimulated emissions of four photons by an atom or molecule with a transition from the ground state $|g\rangle$ to a metastable state $|e\rangle$. The probability of absorption/stimulated emission is chosen to be 50% in each interaction zone by applying the proper laser intensity and interaction time to fulfill the $\pi/2$ condition for the Rabi oscillation. The interaction at the left zone, for example, produces the superposition $(1/\sqrt{2})(|g,0\rangle + |e,+1\rangle \mathrm{e}^{-\mathrm{i}\psi_\mathrm{L}})$ of the molecular states $|e/g,n\rangle$ with a phase ψ_L depending on the laser; n specifies the number of added recoil momenta by the interaction of the laser. The involved transfer of momentum and energy between particle and photon results in a phase shift ϕ of the wave packets, which in closed loops gives rise to an interferometer pattern, that for example can be monitored by the probability P_e of observing a particle in the exited state at the output of the interferometer [3]:

$$P_\mathrm{e} \propto \cos(\phi + \phi_\mathrm{L}) = \cos(2D/v(\Delta \pm \delta) + \phi_\mathrm{L}). \qquad (1)$$

Here $\phi_\mathrm{L} = \Sigma\psi_\mathrm{L}$ denotes the phase transferred from the laser field to the particle in the absorption and emission processes, v the velocity of the particle, D the distance between co-propagating laser beams (see Fig. 1), Δ the detuning of the laser with respect to the transition frequency ν_0 and $\delta = \hbar\mathbf{k}^2/2m$ the photon recoil (+ for the interferometer paths given as dashed lines, − as solid lines). Equation (1) obviously refers to only one velocity class in the ensemble. The presence of a whole velocity distribution leads to a superposition of several interferograms, which are in phase only for $\Delta \pm \delta = 0$. For larger detunings the oscillatory structure of the superimposed interferograms will be washed out, the number of periods observed

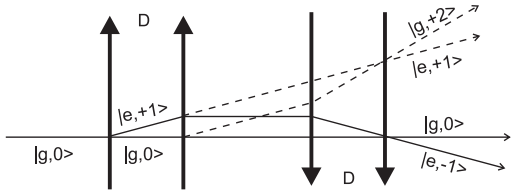

Fig. 1. Scheme of the Ramsey-Bordé interferometer, thin lines show the travelling paths of the molecules, thick lines represent laser beams. Solid lines of wave packets belong to the high frequency recoil component, dashed ones to the low frequency one. The kets give in the first place the electronic state (ground, excited) and in the second the number of transferred photon momenta.

[a] e-mail: tiemann@iqo.uni-hannover.de

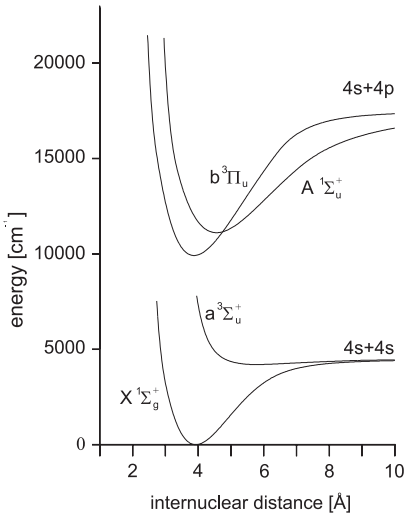

Fig. 2. The lowest electronic states of K_2. The state b is metastable, since transitions to the states X and a are forbidden.

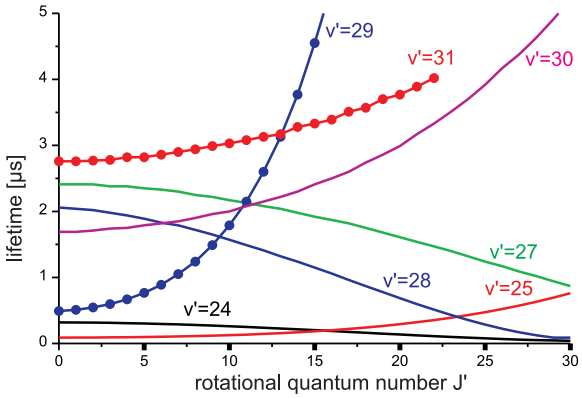

Fig. 3. Lifetimes of selected bands of the 0^+-component $^3\Pi_u$ calculated from equation (3).

by scanning the laser depends on the width of the ensemble's velocity distribution and the lifetime of $|e\rangle$.

2 K_2 in Ramsey-Bordé interferometry

Bordé demonstrated a molecular interferometer with I_2 [6] in the same manner as described in the introduction, while Schmiedmayer *et al.* [7] used Na_2, but applying mechanical gratings as beamsplitter. We choose K_2 for its easy application in a molecular beam and electronic levels to be reached by diode lasers. The potential energy curves of the involved electronic states are shown in Figure 2.

The molecules are excited from the vibrational ground state $v'' = 0$ of X $^1\Sigma_g^+$ to the state b $^3\Pi(0_u^+)$ by laser light around 820 nm [8]. This spin forbidden transition has a small contribution of the transition moment of the A $^1\Sigma_u^+$ state due to spin-orbit coupling [9,10]. The b state is metastable, since dipole transitions to energetically lower states are forbidden due to spin or symmetry arguments. By a partial deperturbation analysis of the states A and b following the formalism also used by Effantin *et al.* [11] for Na_2, we could derive mixing coefficients a and b of the rotational and vibrational levels for both states [8], indicating the amplitudes of the Born-Oppenheimer states for the observed level $\phi_0(J, v)$:

$$|\phi_0(J,v)\rangle = a|^1\Sigma_u^+\rangle + b|^3\Pi(0_u^+)\rangle + ... \qquad (2)$$

The lifetime of the b state is not known to our knowledge. One would expect a lifetime τ_b of the pure b state not shorter than 1 ms. This is about five orders of magnitude larger than that of the A state, which from comparison with other alkali dimers can be assumed to be about $\tau_A = 20{-}22$ ns. To our knowledge this value has not been measured up to now. Knowing the mixing coefficients, one can calculate the lifetime of the $^3\Pi(0_u^+)$ state $\phi_0(J, v)$. Even for states of predominant triplet character, the lifetime is given by the A state admixture because of the large difference in lifetimes of the two states. Thus the decay happens *via* the singlet channel:

$$\frac{1}{\tau_\phi} \propto |\langle \mathrm{X}^1\Sigma_g^+|\mathbf{d}|\phi_0(J,v)\rangle|^2 = |a|^2|\langle \mathrm{X}^1\Sigma_g^+|\mathbf{d}|\mathrm{A}^1\Sigma_u^+\rangle|^2$$

$$\Rightarrow \quad \tau_\phi = \frac{1}{|a|^2}\tau_A \qquad (3)$$

$\mathbf{d}$ is the dipole operator. With $|a|^2 \approx 1.5\%$ of the $J' = 26$ $v' = 27$ level [8], equation (3) leads to a lifetime of 1.3 μs, which will be considered in the present experiment. An experimental check using a linewidth study with saturation spectroscopy in the molecular beam revealed a lower limit for τ_ϕ of 0.5 μs for that level. The good quality of the deperturbation analysis was additionally checked in investigations of the hyperfine structure of selected b state levels [8].

Using the results from the deperturbation analysis, lifetimes for other rovibrational levels of the 0^+ component of the $^3\Pi_u$ can be calculated in this manner. Some selected bands are shown in Figure 3.

3 Experimental setup

For a beam of K_2 potassium metal is evaporated in an oven at 650 K and the vapor expands through a nozzle of 200 μm diameter, which is heated to 700 K to avoid clogging. The beam of K/K_2 propagates through a differential pumping stage and enters an UHV vacuum chamber with a background pressure of 1×10^{-8} mbar. The collimation ratio is 1000, which corresponds to a residual Doppler width in the order of 1 MHz.

In the UHV part of the vacuum system, a typical Ramsey-Bordé-interferometer is built up (*e.g.* [1,3]): the molecules are illuminated by four travelling laser light waves (see Fig. 4). For a satisfactory contrast of the interference signal and since the lifetime of the electronically excited state is in the order of 1 μs (see Sect. 2), the separation D between co-propagating pairs of laser beams should be below 1 mm, assuming velocities of 1000 ms^{-1} in the K_2 beam, in order to avoid high losses of coherence by spontaneous emission.

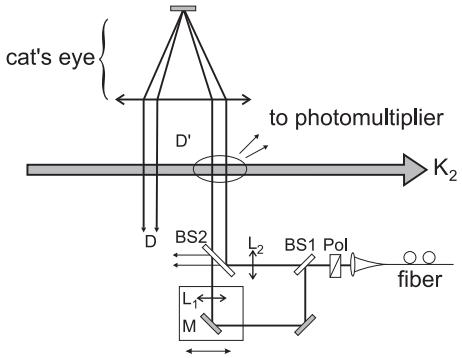

Fig. 4. Optical arrangement to produce the four travelling waves in Ramsey-Bordé geometry. Mirror M and lens L_1 are mounted on a precision translation stage to adjust the zone length D.

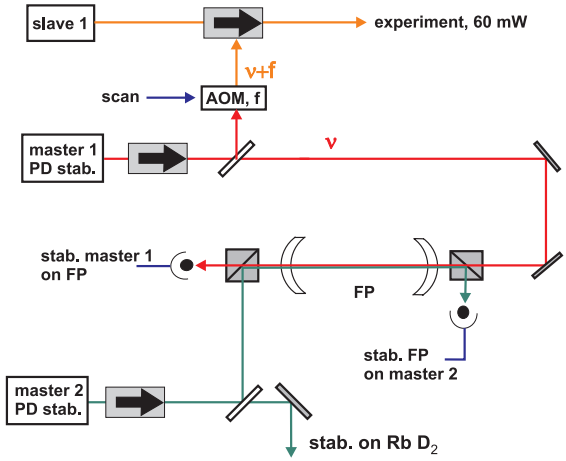

Fig. 5. Scheme of the offset locked laser system used to run the interferometer. For details please refer to Section 3.

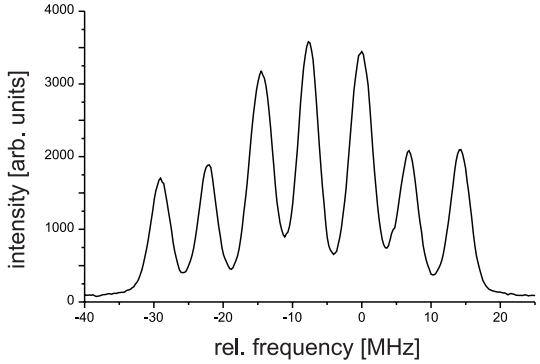

Fig. 6. Scan of the R(25) (27-0) $b^3\Pi(0_u^+) \leftarrow$X with one non-focussed laser beam only.

These laser beams are produced by a 50% beamsplitter BS1 and are focused individually onto the molecular beam with lenses $L_{1,2}$ of $f = 500$ mm focal length, which produce in our case beam diameters of 160 μm. Both laser beams are overlapped on another 50% beamsplitter BS2. The length of the darkzone D is tunable by a stepper motor driven translation stage, which moves mirror M and lens L_1 simultaneously. The second counterpropagating pair of laser beams is produced by reflection with a cat's eye consisting of a mirror and a $f = 300$ mm achromatic lens. The length of the zone D' is chosen to be 1 cm, the travelling time of which guarantees spontaneous decay of all excited molecules. Therefore, only the high frequency (blue) recoil component corresponding to the ground state path in zone D' contributes to the interferometer. The red recoil component would appear at $2\delta \approx 50$ kHz to lower frequencies and could not be resolved with the current setup and signal-to-noise ratio.

At the output of the interferometer the fluorescence is detected by a cooled, red sensitive photomultiplier tube (type Hamamatsu R 943-02). The solid angle of detection is 1.4 srad. Laser straylight is suppressed by a colour glass filter with cut-off for wavelengths $\lambda < 850$ nm (Schott RG 850, 3 mm) and an interference filter with center wavelength of 878 nm and a FWHM of 51 nm.

The light is provided by a laser spectrometer, which is shown in Figure 5. An extended cavity diode laser (ECDL) (master 1) in Littrow configuration is stabilized to a piezoelectrically tunable 1 GHz Fabry-Perot (finesse $F = 150$) by the Pound-Drever method for short term stability. The laser diode is controlled in temperature ($\Delta T \leq 1$ mK) and current ($\Delta I \leq 1\,\mu$A). The sidebands required for Pound-Drever stabilization are produced by modulation of the diode current with 20 MHz. For long term stabilization, this laser is offset locked to a similar system at 780 nm (master 2), which is locked on the Rb D_2 line by saturation spectroscopy. The antisymmetric stabilization signal from Rubidium is obtained by detecting the saturation signal phase sensitively with lock-in technique using the Pound-Drever sidebands. To substract the residual Doppler background of the Rb signal, additionally the pump beam of the saturation setup is chopped: the mixer output is then detected by a second lock-in amplifier on the chopper frequency to obtain the final error signal for the PI servo loop of master 2. The stability transfer between both laser systems is realized by the 150 MHz Fabry-Perot FP stabilized to master 2. Master 1 at 820 nm is shifted by an AOM to interpolate between fringes of the coupling cavity FP. The AOM output drives a slave laser for injection-locking. This also reduces the residual AM introduced by the current modulation (see above). With two such laser systems a beat signal with a FWHM of 30 kHz in one second integration time was observed.

The light is transferred to the vacuum apparatus by a single-mode fiber. The RF frequency of the AOM is controlled by the data acquisition system to allow precise scanning over the transition of interest and averaging of multiple scans.

4 Experimental results

In a first step the fluorescence from a laser scan of the R(25) (27-0) $b(0_u^+) \leftarrow$ X transition with only one interaction zone of 3.6 mm diameter was recorded (Fig. 6). Due to nuclear spin statistics, in this case of odd J'', one observes a hyperfine pattern of seven components due

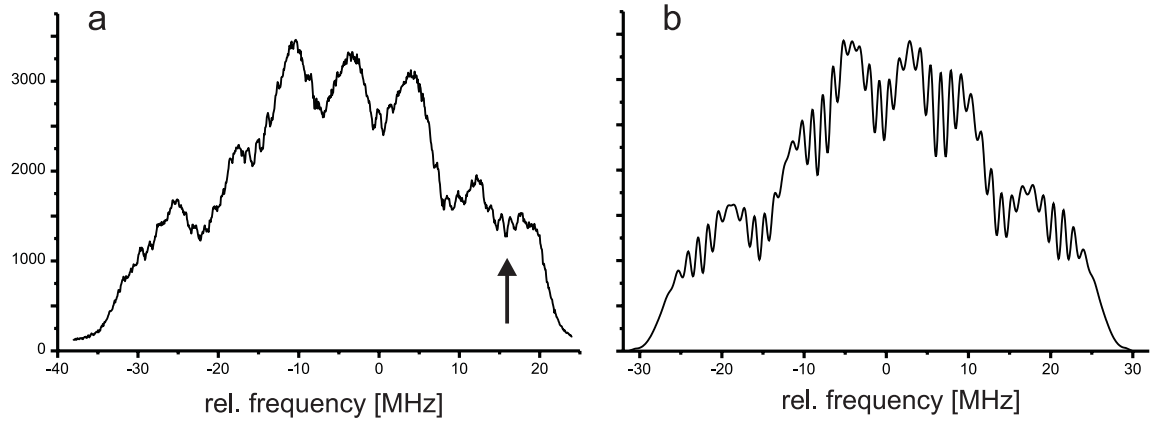

Fig. 7. The R(25) (27-0) b(0_u^+) ← X transition. (a) Four laser beams in Ramsey-Bordé configuration, focused to 160 μm beamdiameter. A high resolution zoom of the region marked by the arrow is shown in Figure 9; (b) simulation of the the same transition with the given experimental parameters.

to the total nuclear spin $I = 3$, which is superimposed by a pattern of three lines from $I = 1$ in the central region of the spectrum. All lines have nearly the same intensity. A more detailed discussion of the hyperfine structure can be found in [8].

Figure 7a shows a scan of the same transition, but now in the Ramsey-Bordé configuration. The laser beams were focused to 160 μm, so that due to transit time broadening single hyperfine components are no longer resolved. Nevertheless one can clearly see interference fringes around the position of each component. Maxima in this scan do not correspond to the peak positions in Figure 6, but are due to overlapping wings of neighbouring components. The distance D was chosen as 350 μm for this scan. A simulation program for the interference structure with the hyperfine multiplet was setup following the formalism introduced in [1]. The basic ideas for the synthesis of the structure are as follows: for J sufficiently large, the hyperfine structure is governed only by transitions with the single selection rule $\Delta F = \Delta J$. F is the quantum number of the total angular momentum $\mathbf{F} = \mathbf{I} + \mathbf{J}$. Therefore, each of the hyperfine lines can be regarded as a separate transition. Furthermore, the interferometer is operated with linearly polarized light, so that the selection rule $\Delta m_F = 0$ holds; thus every hyperfine component consists of $2F'' + 1$ independent interferometers for R transitions ($J'' \rightarrow J'' + 1$). The relative transition probabilities $p(m_{F''})$ within a rotational line are derived with conventional tensor algebra and give an $m_{F''}$ dependence for $\Omega' - \Omega'' = 0$ [13]:

$$p(m_{F''}) \propto (F'' + 1)^2 - m_{F''}^2. \tag{4}$$

Obviously, this leads to transition moments, which differ by a factor of ten for the example of the R(25) line. This makes it impossible to fulfill the $\pi/2$ condition for each m_F with a given laser intensity simultaneously. Deviations from 1/2 transition probability result in a non 50% beamsplitter and in a loss of contrast in the whole interferometer signal. This effect is taken into account in the simulation by summing interferometer signals for all m_F components obtained with transition probabilities calculated with equation (4), while the $\pi/2$ condition is fulfilled only for $m_F'' = 0$ with $F'' = J'' + 3$. The dependence of p by F'' is taken into account by Wigner's $6j$-symbols.

The profile was calculated using the velocity distribution $n(v)$ of K_2 molecules given by the following expression [12]

$$n(v) \propto v^2 \exp\left(-\frac{(v - v_0)^2}{v_{\mathrm{W}}^2}\right) \tag{5}$$

and values for the most probable velocity $v_0 = 912 \pm 30$ ms^{-1} and the velocity width $v_{\mathrm{W}} = 120$ ms^{-1}. These values were derived from measurements with a Doppler detector [12]. Furthermore, a Gaussian shape of the spatial intensity profile of the laser beam was assumed, which introduces an additional loss of contrast in the interferometer signal by molecules passing through regions of lower laser intensity

A simulation for the signal of Figure 7a is shown in Figure 7b. Here the line profiles for each of the ten components were added up, because interferograms are independent from each other. The relative positions of the hyperfine components were taken from the previous hyperfine analysis.

Figures 7a and 7b show rather good agreement: the overall envelope is nicely reproduced. Like in the experimental recording, the interference patterns appear most clearly in the local minima of the simulated spectrum. Even the weak oscillations in the wings of local minima are reproduced by the numerical simulation. The relative contrast of the seven resolved interference patterns shows comparable behaviour in simulation and experiment, *e.g.* the first component on the low frequency side has significantly lower contrast than the third and fifth fringe structure. The lower absolute contrast of the interference fringes in the experimental result with respect to the simulation is probably due to residual misalignment in the experiment and/or phase fluctuations of the laser light. The estimation of the lifetime of $|e\rangle$ introduces only a small uncertainty for the comparison between experimental results and numerical simulations, since we found

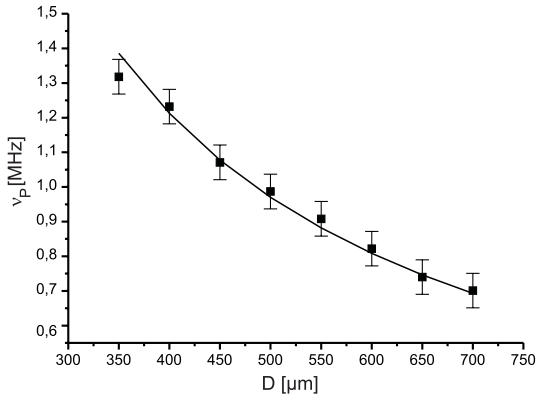

Fig. 8. Measured dependence of the fringe oscillation frequency ν_P on D. The solid line is the theoretical curve according to equation (6) for $v_0 = 970$ ms^{-1}.

by additional simulations, that a decrease of the lifetime of the excited state by a factor of two compared to the calculated 1.3 μs does not decrease the contrast more than 30%.

A variation of the distance D results in a change of interference fringe frequency ν_P according to equation (1)

$$\nu_P = \frac{v_0}{2D} \cdot \tag{6}$$

Systematic measurements of this variation as function of the distance D are shown in Figure 8. The interference fringe frequencies were determined by substracting the incoherent background signal (locally fitted to a polynomial of 4th order) from the data and then Fourier transforming these oscillatory structures. Figure 9 shows scans with substracted background for $D = 400$ and 700 μm. Solid lines are simulated fringes without incoherent background, summed only over the experimental velocity distribution ($v_0 = 970$ ms^{-1}, $v_W = 120$ ms^{-1}). The amplitude of the simulated fringe is adjusted to the experimental one. The errors given in Figure 8 are due to the uncertainty of determining the maxima in the FFT traces.

The solid line in Figure 8 represents the theoretical values of ν_P according to equation (6) for $v_0 = 970$ ms^{-1}. It has to be mentioned, that the most probable velocity v_0 shows a slight variation from day to day. We think this is caused by the limited reproducibility of setting the oven temperature, which influences the K/K_2 vapor pressure, under which the molecules expand into the vacuum. Applying a seeded beam will probably improve the stability of the system in this respect. The data in Figure 8 are obtained in one day of measurement under fixed experimental conditions. The absolute values of D have a systematic error of $\pm 40\,\mu$m, because of the uncertainty of adjusting the overlap of the laser beams for $D = 0$. The relative distances are determined much better by the good mechanical layout of the translation stage.

The quality of the observed spectra in Figure 9 show the capability of the present experimental setup to determine small phase shifts in the interference pattern very accurately, which can be induced by collisions or external

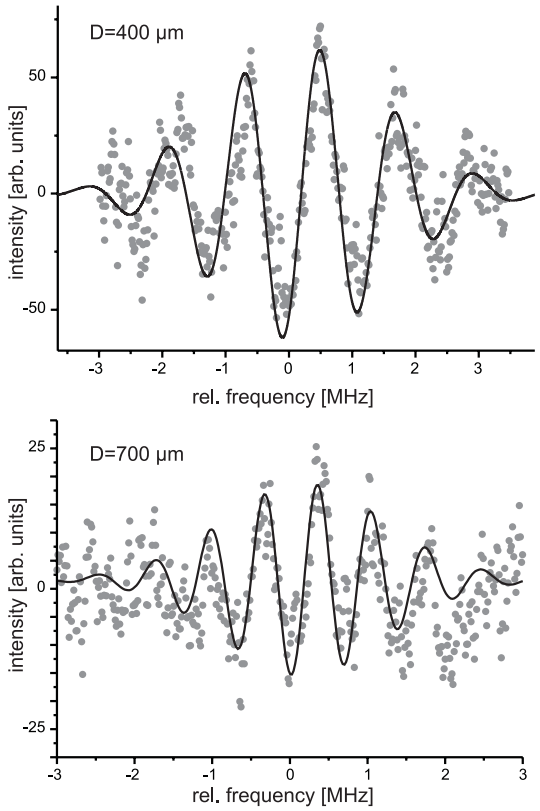

Fig. 9. Fringes with substracted incoherent background. The time constant for recording was 150 ms. 16 scans for $D = 400\,\mu$m and 26 for $D = 700\,\mu$m were averaged. Solid lines show simulations for the experimental conditions (see text). The cumulated phase ϕ_L in equation (1) was fixed to 1.5 rad.

fields or other interactions on the path within the interferometer. Fitting an oscillation $I(\nu)$ damped by a Gaussian envelope

$$I(\nu) = A \exp\left(-\frac{(\nu-\nu_0)^2}{\nu_W^2}\right) \cos\left(\frac{2\pi}{\nu_P}(\nu-\nu_0)+\phi\right) \tag{7}$$

to the traces in Figure 9, one can determine the phase ϕ with an uncertainty of 25 mrad ($D = 400\,\mu$m) and 55 mrad ($D = 700\,\mu$m).

5 Conclusion and outlook

We have demonstrated and characterized a Ramsey-Bordé interferometer with K_2 using very weak perturbations between the two states A $^1\Sigma_u^+$ and b $^3\Pi(0_u^+)$. Such perturbations appear in many molecular spectra and may open the possibility of matter wave interferometry with a large number of different molecules.

The measured spectra as well as the dependence of fringe oscillation frequency ν_P on the dark zone length D are in good agreement with numerical simulations we performed. Due to the μs lifetime of the excited state, high resolution spectroscopy with kHz resolution or better seems not to be the most promising goals, as *e.g.* intercombination lines in alkaline earth atoms. But the K_2

wave packet can be used as a sensitive detector for phase changing influences. Any effect influencing the evolution of the matter wave differently in both quantum states involved will result in a phase shift of the observed fringe pattern. For example, we started to investigate the influence of collisions between the K atoms in the beam and the "sensor" molecules. Collision induced phase shifts were already subject of experiments with atoms [7] as well as with molecules [14]. In our experiment, in contrast to these two experiments, firstly we will observe the collisional influence on selected quantum states of the molecular collision partner and secondly, the collisions will take place between particles *within* the beam. Applying a supersonic beam with seed gas, the relative velocities of the collision partners can be in the order of 10 ms^{-1} corresponding to translational energies around one Kelvin, which is a cold collision situation. In these experiments modulation techniques to simplify the overlapping structures of the hyperfine multiplet will be helpful. Further experiments are possible by manipulation of the colliding atoms, *e.g.* exciting them to Rydberg states and in this way changing the long range van der Waals interaction between the collision partners, which is proportional to the polarizability of the involved species. Another method is to switch K–K_2 collisions on and off by deflecting the atoms out of the beam by a resonant laser field. The long term goal may be the analysis of collisions involving molecules excited near the dissociation limit. The access to those levels is possible from the bound molecule. This was demonstrated with experiments on Na_2 [15,16]. Such experiments can provide new data about three body collision processes, which are of interest in cold dense atomic ensembles.

This work was supported by the Deutsche Forschungsgemeinschaft (SFB 407).

References

1. Ch.J. Bordé, Ch. Salomon, S. Avrillier, A. van Lerberghe, Ch. Bréant, D. Bassi, G. Scoles, Phys. Rev. A **30**, 1836 (1984).
2. Ch.J. Bordé, Phys. Lett. A **140**, 10 (1989).
3. U. Sterr, K. Sengstock, J.H. Müller, D. Bettermann, W. Ertmer, Appl. Phys. B **54**, 341 (1992).
4. J. Helmcke, D. Zevgolis, B.Ü. Yen, Appl. Phys. B **28**, 83 (1982).
5. Ch.J. Bordé, S. Avrillier, A. van Lerberghe, Ch. Salomon, Ch. Bréant, D. Bassi, G. Scoles, Appl. Phys. B **28**, 82 (1982).
6. Ch.J. Bordé, N. Courtier, F. du Burck, A.N. Goncharov, M. Gorlicki, Phys. Lett. A **188**, 187 (1994).
7. J. Schmiedmayer, M. Chapman, C. Ekstrom, T. Hammond, S. Wehinger, D. Pritchard, Phys. Rev. Lett. **74**, 1043 (1995).
8. Ch. Lisdat, H. Knöckel, E. Tiemann, J. Mol. Spec. **199**, 81 (2000).
9. A. Ross, P. Crozet, C. Effantin, J. d'Incan, R.F. Barrow, J. Phys. B **20**, 6225 (1987).
10. G. Jong, L. Li, T.-J. Whang, W. Stwalley, J. Coxon, M. Li, A. Lyyra, J. Mol. Spec. **155**, 115 (1992).
11. C. Effantin, O. Babaky, K. Hussein, J. d'Incan, R. Barrow, J. Phys. B **18**, 4077 (1985).
12. G. Scoles, *Atomic and molecular beam methods* (Oxford University Press, 1988) p. 227
13. A.R. Edmonds, *Angular momentum in quantum mechanics* (Princeton University Press, 1964).
14. M. Chapman, C. Ekstrom, T. Hammond, R. Rubenstein, J. Schmiedmayer, S. Wehinger, D. Pritchard, Phys. Rev. Lett. **74**, 4783 (1995).
15. M. Elbs, H. Knöckel, T. Laue, C. Samuelis, E. Tiemann, Phys. Rev. A **59**, 3665 (1999).
16. E. Tiemann, H. Knöckel, H. Richling, Z. Phys. D **37**, 323 (1996).